

Non-invasive Imaging Correlates with Histological and Molecular Characteristics of an Osteosarcoma Model: Application for Early Detection and Follow-up of MDR Phenotype

A. DUTOUR^{1,5}, D. LECLERS¹, J. MONTEIL², F. PARAF³,
J.L. CHARISSOUX⁴, R. ROUSSEAU⁵ and M. RIGAUD^{1*}

Departments of ¹Medical Biochemistry, ²Nuclear Medicine, ³Pathology and,
⁴Orthopedic Surgery, School of Medicine, University of Limoges;
⁵Oncologie Pédiatrique, Centre Léon Bérard, Lyon, France

Abstract. *Background:* In an orthotopic rat osteosarcoma model, histological and molecular findings were compared with the results of non-invasive imaging methods to assess disease progression at the primary site, the pattern of metastatic dissemination and the chemoresistance phenotype. *Materials and Methods:* Primary tumor engraftment, vascularization, growth and metastatic spread were evaluated using ¹⁸F¹⁸FDG tomoscintigraphy. Bone neof ormation in the primary tumor and metastasis was determined using ¹⁸F¹⁸Na confirmed by classical histological studies. Chemoresistance phenotype was assessed by analysis of *MDR1* and *MRP1* genes expression compared to ^{99m}Tc MIBI imaging. *Results:* ^{99m}Tc MIBI imaging correlated with the overexpression of the *MDR1* and *MRP1* genes. ¹⁸F¹⁸FDG, ¹⁸F¹⁸Na and ^{99m}Tc tomoscintigraphies revealed that the pattern of vascularization, bone neof ormation and hematogeneous metastatic dissemination in our animal model mimics its human counterpart. *Conclusion:* Multimodality, non-invasive imaging is a valid surrogate marker of histological and molecular characteristics in an orthotopic osteosarcoma model in immunocompetent rats; it allows extensive *in vivo* follow-up of osteosarcoma, including longitudinal analysis of chemoresistance.

Osteosarcoma is the most frequent primary malignant bone tumor in children and adolescents despite accounting for only 0.1% of all tumors in this age group (1). Although the

Correspondence to: Professor Michel Rigaud, Department of Medical Biochemistry, School of Medicine, University of Limoges, 2 rue du Dr Raymond Marcland 87042, Limoges, France. Tel: +33 5 55 05 63 41, e-mail: rigaud.michel@yahoo.fr

Key Words: Osteosarcoma, syngeneic model, tomoscintigraphy, PET-scan, multidrug resistance.

prognosis of osteosarcoma has greatly improved over the last two decades with the addition of neoadjuvant and adjuvant chemotherapy, there is still a need for efficient therapeutic alternatives for non-responders, relapsed patients and patients with metastasis. In fact, more than 30% of patients with osteosarcoma will succumb to metastatic disease (2).

A better understanding of the biology of osteosarcoma at the molecular level has allowed new therapeutic strategies to be designed. *In vitro* models for the evaluation of new therapeutic modalities have been developed (3, 4), but they are of limited value since they usually fail to reproduce the complex interactions of a tumor with its microenvironment (5). Consequently, agents that have shown promising therapeutic effects *in vitro* often fail to do so when administered *in vivo* in tumor models (6, 7). Hence, new therapeutic modalities should ideally be evaluated in a relevant animal tumor model before going into human clinical trials.

An ideal osteosarcoma animal model should be syngeneic, grow at orthotopic site, have a metastatic potential and be highly reproducible. Most osteosarcoma models currently available do not meet all these criteria. Most are xenotransplants models in immunocompromised animals (8-10). Only few models are syngeneic, usually carcinogen- or radio-induced; they usually grow at heterotopic sites (11, 12). Canine osteosarcoma is a pertinent model since it is both syngeneic and orthotopic but the availability of canine agents limits the extent of this naturally occurring tumor model.

The value of the multidrug resistance genes *MDR1* and *MRP1* as prognostic factors has been suggested in osteosarcoma (13). The products of these two genes, Pgp for *MDR1* and MRP for *MRP1*, belong to the ATP binding cassette superfamily of membrane transporter proteins (14, 15). Both proteins act as energy-dependent efflux pumps that convey cytotoxic drugs and radioactive markers such as

Table I. Primers and PCR-amplified fragments for analysis of MDR1 and MRP1 expression by RT-PCR.

Primers	Size of amplified fragment	Sequence amplified	Accession number
Fw: CGCCATGGATGACGATATCGC Rv: CTCCGGAGTCCATCACAATGC Tm: 56°C	472 bp	Beta Actin	NM 031144 (23)
Fw: CTGGCTTGGTGTGAACTGAT Rv: AGGCTCTGGCTTGGCTCTAT Tm: 53°C	394 pb	MRP 1	X 96394 (22)
Fw: GGACAGAAACAGAGGATCGC Rv: CCCGTCTTGATCATGTGGCC Tm: 55°C	440 bp	MDR 1a	S66618 (23)
Fw: GAAATAATGCTTATGAATCCCAAAG Rv: GGTTTCATGGTCGTCTCTTGA Tm: 56°C	326 bp	MDR 1b	S66618 (23)

Fw: forward primer, Rv: reverse primer, Tm: melting temperature.

^{99m}Tc Sestamibi (^{99m}Tc MIBI) out of tumor cells (16). In our institution, we have an orthotopic osteosarcoma model established in immunocompetent rats. We have previously used this model to evaluate the therapeutic efficiency of suicide-gene and antiangiogenic-gene therapy approaches (6, 17, 18). In this study, we described the morphological, histological and molecular characteristics of this model, using conventional analyses (immunohistology and molecular methods) and non-invasive imaging studies: we evaluated the possibility of using multimodality-imaging techniques to analyse, in an *in vivo* and real-time non-invasive manner, the evolution of a primary tumor, apparition of metastases, the determination and longitudinal evolution of chemoresistance phenotype. If we can show that multimodality-imaging studies adequately correlate with the conventional, more invasive analysis methods, this would allow for design of preclinical therapeutic approaches that require fewer animals given that the follow-up of tumor response and the evolution of chemoresistance phenotype could be done without the need to euthanize animals.

Materials and Methods

Tumor model and treatment. All surgical procedures and care given to animals were performed according to institutional and national guidelines. Surgical procedures were conducted under general anesthesia with isoflurane/oxygen (2.5%/2.5%) dispensed by an anaesthesia apparatus (Minerve, Esternay, France). Three independent series of 21- to 28-day-old Sprague-Dawley rats (Centre d'élevage Depré, St Doulchard, France) were used in this study. The orthotopic osteosarcoma used was initially established by local injection of colloidal radioactive ¹⁴⁴Cerium (19) and a transplantable tumor was obtained from this radio-induced tumor (20). Small fragments (50 mm³) sampled from the hyperproliferative osteogenic area were grafted in a paratibial position into the left posterior leg of rats after periostic abrasion. When tumor ¹⁸FDG uptake reached 4% of the whole body

fixation, the animals were randomly divided into two groups of 10 animals each, one control and one methotrexate-treated group. The chemotherapy-treated group received a weekly intraperitoneal injection of methotrexate at a dosis of 0.25 mg/kg (Sanofi-Aventis, Paris, France) over a period of 4 weeks. The control group received at the same frequency intraperitoneal injections of physiological serum. The study was conducted over 35 days. Tumors were measured twice weekly throughout the study, and the volume calculated using the formula established by Carlsson ($V=0.5x \times b^2$ where a is the largest diameter measured and b the smallest) (21). All animals were euthanized if they showed any sign of distress or when the orthotopic tumor reached 20 ± 2 cm³. At the time of necropsy, tumors, lungs, liver, heart and skeletal muscle were collected for RT-PCR assays and/or histological examinations.

RT-PCR for the determination of multidrug-resistance genes expression. Total RNA was extracted from disrupted tissues (primary tumor, lung, lung metastases, skeletal muscle, cardiac muscle, liver) using an RNeasy® mini kit, (Qiagen, Courtaboeuf, France) according to the manufacturer's instructions. cDNA amplification was obtained by RT-PCR on 5 µg of RNA using the Omniscript® RT kit (Qiagen), specific sets of primers for each gene and the AmpliTaqGold® Taq DNA polymerase (Applied Biosystems, Foster City, CA, USA). β-actin was used as a control to which the expression of *MDR1* and *MRP1* genes was normalized. Primer sequences and length of PCR products are shown in Table I (22, 23). PCR products were separated by electrophoresis on a 1% agarose gel and visualized under UV light in the presence of ethidium bromide. Semiquantitative gene-expression analyses were performed using a Kodak Image Station and corresponding software (Kodak, New Haven, CT, USA).

Pathology. Tumors and lungs were fixed in 10% formalin. Paraffin-embedded tumor sections (8 µm) were stained using hematoxylin-eosin saffron (HES). Triple immunohistochemical staining for endothelial and apoptotic cell detection was performed on frozen sections blocked with 5% goat serum (Chemicon, Temecula, CA, USA). Endothelial cells were stained with RECA-1 primary antibody (1/400; Serotec, Oxford, UK) and Cy3-goat anti-mouse IgG as secondary antibody (1/400; Jackson

Immunoresearch, West Grove, PA, USA). Apoptotic cells were detected by terminal deoxynucleotidyl transferase-mediated (dUTP) biotin nick end labeling (TUNEL) (*In Situ* Cell Death Detection Kit, Roche, Mannheim, Germany) and 4',6-diamidino-2-phenylindole dihydrochloride (DAPI) (Sigma Aldrich, St Louis, MO, USA) (1 µg/mL in PBS).

Imaging studies. Imaging studies were performed weekly on all animals. *In vivo* functional and metabolic imaging studies were performed using ¹⁸FDG (fluorodeoxyglucose) coincidence detection emission tomography (¹⁸FDG CDET) and technetium 99m methoxyisobutylisonitrile (^{99m}Tc-MIBI) scintigraphy. The ^{99m}Tc-MIBI scintigraphy was performed 48 h after ¹⁸FDG CDET

After fasting for 6 h, animals were injected intravenously with 92 MBq/kg of ¹⁸FDG (Flucis, Shering/Cis-bio International, Gif-sur-Yvette, France). Tomographies were performed 5 h after the intravenous injection using a double-head gamma camera (Axis, Philips Medical Systems, WA, USA). Following a 30-minute bidimensional acquisition consisting of 30 steps every 6°, data were processed without attenuation correction and images were reconstructed using an iterative method (EMML: 20 iterations). ¹⁸FDG uptake was defined as the ratio between the tumor radioactivity within the tumor mass compared to the whole body total radioactivity detected in the 5-cm thickness coronal slice (tumor uptake = tumor radioactivity/total radioactivity). Acquisition was performed immediately after the intravenous injection of 370 MBq/kg of ^{99m}Tc-MIBI. Sixty-minute imaging static acquisition was obtained from anesthetized rats laying on the gamma camera (DSX, Sopha Medical, France). Tumor ^{99m}Tc-MIBI uptake index was defined as the ratio between tumor and whole body radioactivity. Acquisition was performed 5 h after an intravenous injection of 370 MBq/kg of ¹⁸FNa. Sixty-minute image acquisition was conducted using a gamma camera similarly to ¹⁸FDG acquisition.

Statistical analysis. All data are presented as means ± SEM. Differences from the mean were tested for significance by means of the Student's *t*-test using Statview Software. The level of statistical significance was set at *p* < 0.05.

Results

¹⁸FDG uptake (¹⁸FDG CDET) correlates with primary tumor growth. Tumor engraftment at the primary site of implantation occurred in more than 95% of the animals. The primary tumor progressed rapidly from the time of implantation: after seven days, a primary tumor could readily be detected by physical palpation in 98% of transplanted animals. The mean tumor volume significantly increased from 0.23 ± 0.05 cm³ at day 7 to 20.5 ± 2.263 cm³ at day 35 (*p* < 0.01) (Figure 1A). These physical findings correlated with ¹⁸FDG uptake (Figure 1A and 1B) with uptake as low as 3 ± 1% at day 7 if the tumor was palpable up to 36 ± 7% of whole body fixation at day 35 (*p* < 0.01) (Figure 1B) with a mean tumor volume measured at 20.5 cm³ (range from 17.5 to 24.25 cm³). ¹⁸FDG uptake in the controlateral paw did not change throughout the study.

¹⁸FNa uptake corroborates osteogenesis of the primary tumor. Preferential uptake of ¹⁸FNa in newly mineralized bones correlates with bone formation. ¹⁸FNa imaging performed 4 weeks after tumor implantation revealed heterogeneity of primary tumors with differentially stained areas, the center of the tumor appearing unstained while an intense uptake was observed at its periphery (Figure 2A). These scintigraphic findings were confirmed histologically, the periphery of the tumor appearing mineralized with signs of hyperproliferation: high cell density, increased mitotic index, bulky irregular nuclei with frequent nucleoli (Figure 2B). In sharp contrast, the central portion of the tumor often appeared clearly necrotic with numerous microcalcifications and areas of viable proliferating tumor cells forming a vessel-centered ring (Figure 2C).

Vascular spread is the preferred route of metastatic dissemination. Endothelial cells staining with RECA-1 antibody revealed dense vascularization consisting of normal and irregular vessels forming clusters of high vascular density whereas other parts of the tumor lacked any vessels (Figure 3A). The vascular density was the highest at the hyperproliferative periphery of the tumors. This anarchic vascular structure is typical of osteosarcoma in humans, particularly in highly aggressive tumors. Only few apoptotic tumor cells were detected by TUNEL staining confirming the aggressivity of the tumor (Figure 3B).

¹⁸FDG uptake (¹⁸FDG CDET) reveals early metastatic spread. Pulmonary metastases (≥ 4 mm in diameter) were detected by ¹⁸FDG as early as 3 weeks after tumor implantation (Figure 1B). The presence of these metastases was confirmed by histological examination of euthanized animals 24 hours after imaging. Five weeks after tumor implantation, all the animals had lung metastases, many of them being macroscopically visible on pathological examination reaching up to 1 cm in diameter (Figure 4A). Histologically, metastases consisted of densely packed large malignant mesenchymal cells similar to those seen in the primary tumor (Figure 4). In the largest metastases, necrotic areas representing 10% of the tumor could be found in the middle of the metastases. Metastases were also detected by ¹⁸FNa imaging, (Figure 2A); an intense uptake of this radionuclide at the lung site correlated with the formation of osteoid at the periphery of these metastases, as confirmed by classical HES staining (Figure 4A). These observations confirmed the aggressiveness of the metastases spreading from the primary tumor, a characteristic also observed in human osteosarcoma.

^{99m}Tc-MIBI uptake is related to the multi-drug resistance phenotype. ^{99m}Tc-MIBI scans were performed on a weekly basis over the study, the first two days after tumor first

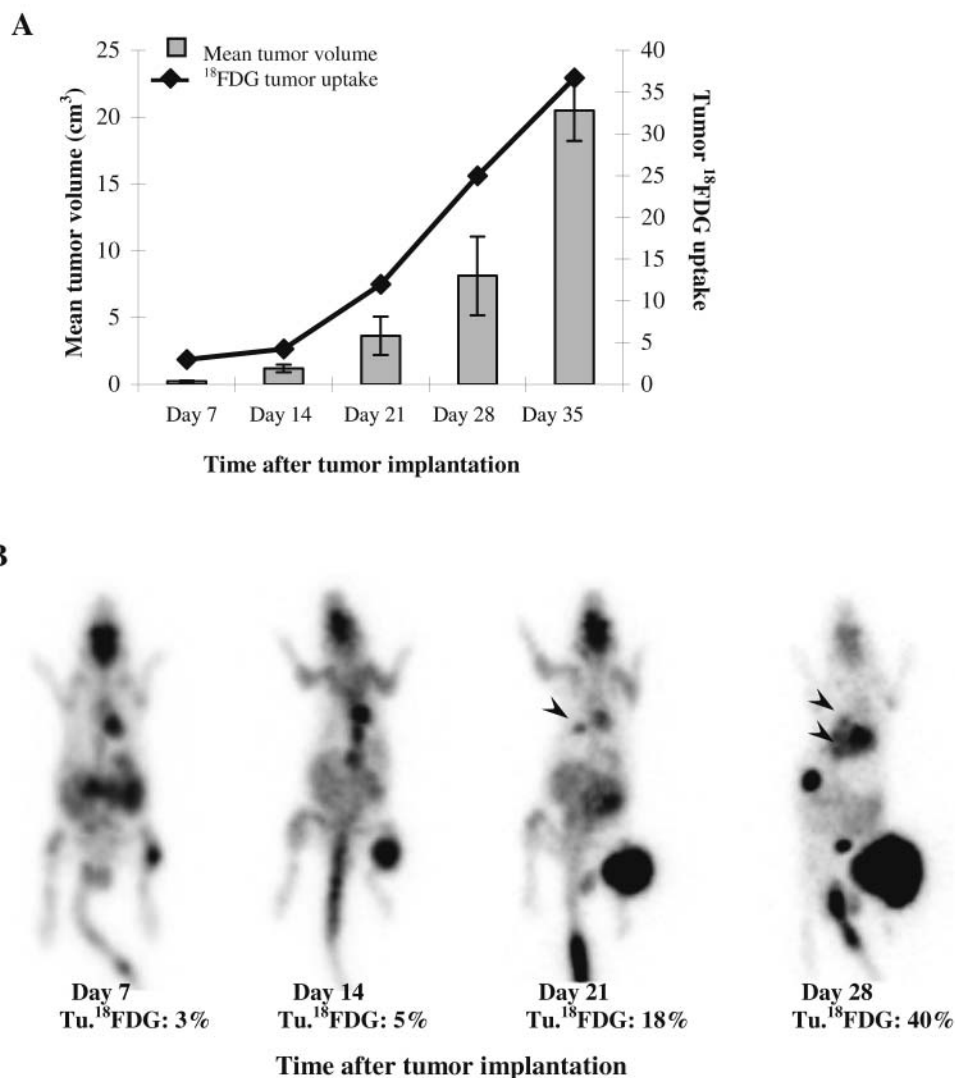


Figure 1. (A) ¹⁸F-FDG tumor uptake correlated to tumor volume. The histograms represent the mean tumor volume calculated by Carlson's formula. The line shows the evolution of ¹⁸F-FDG tumor uptake. Primary tumor volume increased rapidly from 0.23 cm³ to 20.5 cm³ 5 weeks after tumor implantation. Meanwhile ¹⁸F-FDG tumor uptake increased from 3 to 36.71%. Bars indicate standard deviation. (B) ¹⁸F-FDG CDET imaging of primary tumor progression. Tu. ¹⁸F-FDG indicates ¹⁸F-FDG uptake by the tumor expressed as a percentage of the whole body radionuclide fixation. Primary tumors grew fast as shown by the rapid increase in ¹⁸F-FDG uptake (from 3% to 36%). Pulmonary metastases (arrowheads) could be detected 21 days after tumor implantation.

detection by ¹⁸F-FDG CDET. ^{99m}Tc-MIBI scans did not reveal any increased uptake of the radionuclide at the primary tumor site compared to the contralateral healthy paw (Figure 5A). This absence of ^{99m}Tc-MIBI uptake was maintained over time (Figure 5A) and was due to the rejection of the tracer by the transporter proteins, Pgp and MRP1. The expression of these proteins by the tumor cells were confirmed by RT-PCR.

RT-PCR on organs 24 h after ^{99m}Tc-MIBI imaging revealed variable *MDR1* and *MRP1* gene expression with levels ranging from undetectable to high (Figure 5B).

MDR1 isoforms showed selective tissue distribution with the *MDR1a* and *MDR1b* isoforms being expressed in the heart, primary tumor and lung metastases (Figure 5B). When normalized to β -actin expression, *MDR1* and *MRP1* gene expression appeared overexpressed in the primary tumor as well as lung metastases (a 2.1-fold expression of the *MDR1* isoforms and a 1.8-fold overexpression of *MRP1*, respectively) thus correlating with the absence of tumor fixation of ^{99m}Tc MIBI. As soon as the tumor could be detected, expression of both *MDR1* isoforms and *MRP1* was evident in the tumor. This observation shows that the

chemoresistant phenotype of the rat osteosarcoma model is not induced by chemotherapy.

Whereas the expression of *MDR1* isoforms and *MRP1* by tumor cells did not change over time (Figure 5A, B), it was altered by chemotherapy. The group of rats treated by 4 courses of methotrexate chemotherapy presented an increase in *MDR1* and *MRP1* tumor expression as shown by RT-PCR. A 2.4-fold expression of *MDR1a*, 2.6 fold of *MDR1b* and 1.9-fold of *MRP1* were observed (Figure 5D) in comparison to the expression level of these genes at the same time point in the untreated group (Figure 5B). This increase is characterized by the same absence of tumor uptake of ^{99m}Tc MIBI that was observed over time (Figure 5C). It is of note that methotrexate did not significantly inhibit primary tumor growth as assessed by tumor volume evolution (Figure 6), the mean tumor volume of the treated group reaching 21.8 cm³ whereas the mean tumor volume of the control group was 21 cm³ ($p>0.05$).

Discussion

Despite the improvements in chemotherapeutic regimens over the last two decades, the 5-year survival rate of osteosarcoma patients has remained stable (55%-70%) (24). This clearly shows that there is a need for new therapeutic approaches for osteosarcoma treatment. To assess new strategies, relevant preclinical animal models and clinically relevant follow-up methods are needed. Using non-invasive imaging methods, we describe an orthotopic rat osteosarcoma model mimicking the human one, hereby showing the validity of these methods in following-up tumor evolution and its histological and phenotypic features.

While several animal models of osteosarcoma have been developed over the years, few of them are tumorigenic and metastatic (25-27). Among the remaining, even fewer are established in immunocompetent animals (28, 29); to our knowledge, only two other models show these characteristics (28). Here we described the characteristics of a highly reproducible rat osteosarcoma model that meets most, if not all, of the requirements of a preclinical model: reproducibility, primary tumor growth, metastatic potential, tumor histological and phenotypic features. Similarly to human osteosarcoma, our syngeneic orthotopic osteosarcoma model in immunocompetent rats showed evidence of bone invasion, osteoid formation and high tumor angiogenesis, all indicators of tumor malignancy predictive of metastatic potential (30, 31) and consistent with hematogeneous spreading similar to human osteosarcoma (1). The high growth rate at the primary site resulted in morbidity as early as 28 days following the implantation of tumor fragments. As evidenced by ^{18}F FDG imaging, the primary tumor had a high glucose metabolism that correlated with rapid growth, invasiveness and

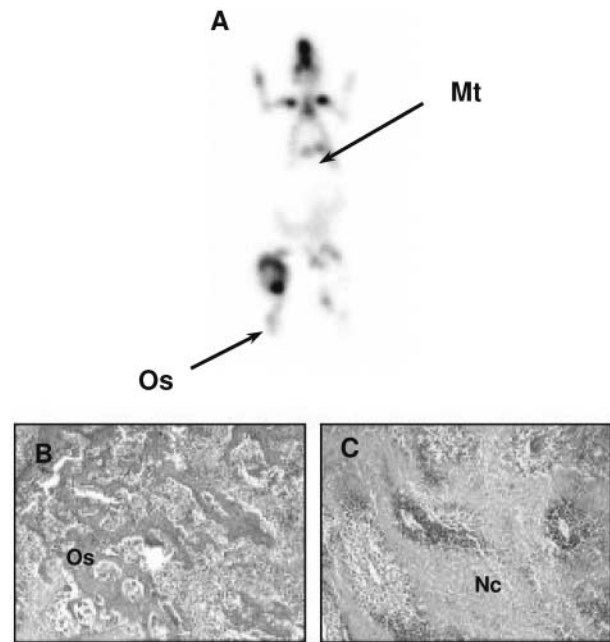


Figure 2. (A) ^{18}F Na tomoscintigraphy allows the detection of viable newly mineralised (black stained) and necrotic (gray) areas within the tumor. ^{18}F is mainly incorporated at the periphery of the tumor, in the osteoid-forming zones (Os). Pulmonary metastases could also be detected (Mt). (B, C) Histological staining of the primary tumor (HES staining) indicating (B) hyperproliferative areas characterized by a high cellular density and formation of osteoid structures (darker trabeculae; Os) and a (C) necrotic central area (Nc) where rings of proliferative cells surrounding a vessel are found. Original magnification $\times 100$.

metastatic spread to the lungs. The imaging methods, confirmed by classical histological and molecular analyses, enabled us to establish that the pulmonary metastases present the same phenotypic and histological characteristics as the primary tumor cells, showing that osteosarcoma cells are as aggressive in the primary tumor as they are in the lung metastases.

RT-PCR, corroborated by ^{99m}Tc -MIBI imaging, established that *MDR1* and *MRP1* were overexpressed in the primary tumor and in the pulmonary metastases. Overexpression of these genes is associated, in different tumors, with resistance to standard chemotherapy and excretion of radiotracer ^{99m}Tc MIBI, two characteristics presented by our model. Multidrug resistance associated with overexpression of *MDR1* and *MRP1* genes is a major problem in the treatment of osteosarcoma (16, 32, 33). Moreover, we showed that primary tumor expression of *MDR1* and *MRP1* increases under chemotherapeutic treatment, a fact often found in human tumors (34). In patients with osteosarcoma, *MDR1* overexpression at diagnosis correlates with resistance to chemotherapy and is an important adverse prognostic factor (35). We clearly show that ^{99m}Tc MIBI imaging has a role in the early detection of MDR

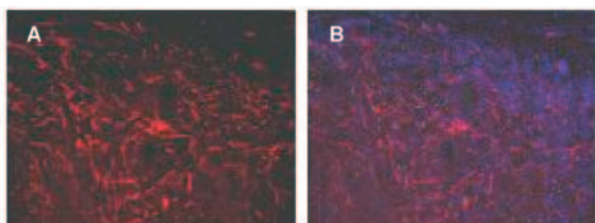


Figure 3. (A) RECA-1 immunostaining demonstrated enhanced vascularization in the primary tumor. Vessels are numerous, irregular and form areas of higher vascular density. (B) In the highly vascularized area, only few apoptotic tumor cells, positive for TUNEL and DAPI, were detected. Original magnification x50.

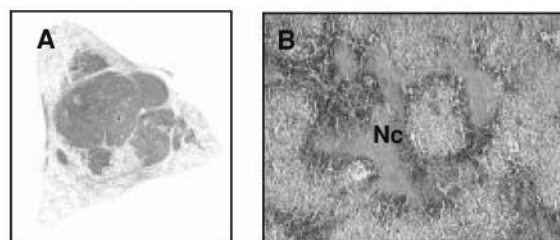


Figure 4. Pulmonary tissue 4 weeks after tumor implantation (HES coloration). (A) Macroscopic metastases could be seen, the largest reaching 0.8 cm to 1 cm in diameter. (B) Histologically, the metastases were identical to the primary tumor, with high cellular density and necrotic areas (Nc). Original magnification x100.

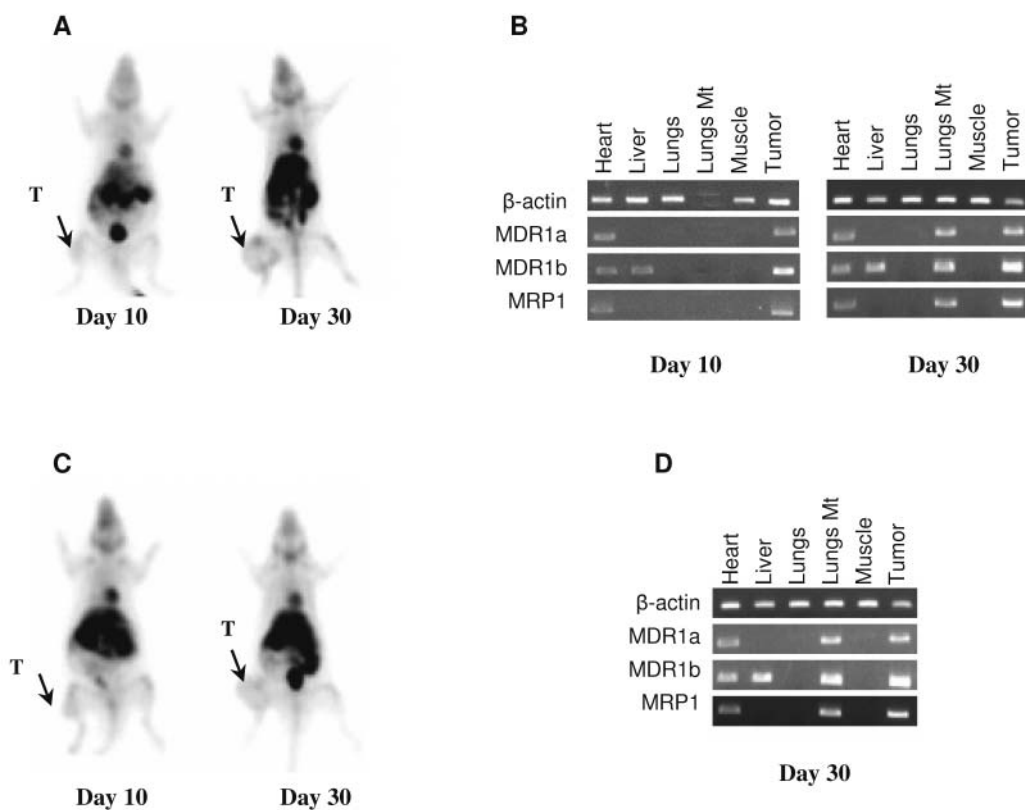


Figure 5. MDR1 and MRP1 gene expression determined by ^{99m}Tc-MIBI tomoscintigraphy and RT-PCR in the primary tumor and other organs (B-D). (A) The primary tumor (T) showed a weak signal on ^{99m}Tc-MIBI tomoscintigraphy performed 10 days after tumor implantation. This absence of tumor uptake of ^{99m}Tc-MIBI, consistent with the tumor overexpression of the MDR1 and MRP1 genes, was maintained over time. (B) RT-PCR performed on tumor and control tissues confirmed tumor overexpression of MDR1 and MRP1 in the primary tumor and in the pulmonary metastases (2-fold overexpression of MDR1 isoforms and 1.8-fold of MRP1). (C, D) Standard chemotherapy course did not affect MDR1 and MRP1 expression. (C) After 4 courses of methotrexate, no tumoral uptake of ^{99m}Tc-MIBI could be observed. (D) The RT-PCR revealed an increase in the expression of MDR1 and MRP1 (a 2.4- and 2.6-fold increase compared to the untreated group, respectively).

phenotype of osteosarcoma and could therefore be useful for the early identification of non-responders, or the evaluation of chemosensitisers *in vivo* in preclinical animal models and ultimately in patients (16, 36, 37).

The originality of our study resides in the use of non-invasive imaging methods to monitor disease progression and chemoresistance *in vivo* without the classical limitations of animal euthanasia to analyze tumor histology and

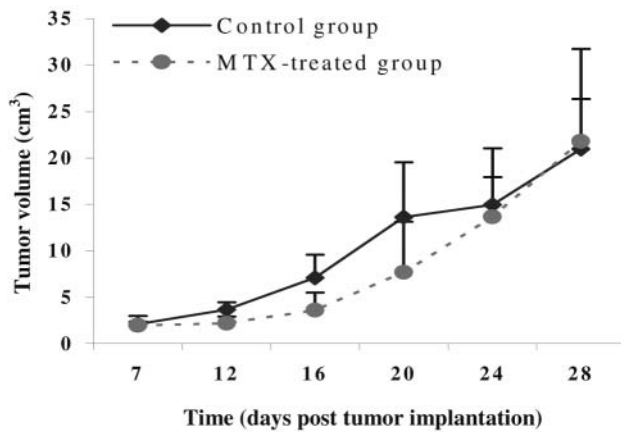


Figure 6. Tumor volume evolution under methotrexate treatment. The tumor volume was calculated bi-weekly using Carlson's formula. No significant inhibition of tumor growth could be observed in the methotrexate-treated group ($p > 0.05$). Bars indicate standard deviation.

determine metastasis emergence. The correlation between tumor volume and tumor ^{18}F FDG uptake has been described for several tumor types (38) and reinforces the validity of ^{18}F FDG tomoscintigraphy as an early, non-invasive metabolic predictor for tumor response before any gross morphological changes occur (18, 38-40). These findings, along with our current results, confirm our previous study in rats where we showed that osteosarcoma regression can be detected by ^{18}F FDG before any morphological changes could be noticed and that ^{18}F FDG uptake is the most significantly negative prognosis factor (18, 38). ^{18}F FDG is incorporated only into viable cells. Hence, it can also distinguish between necrotic and viable areas and may represent an important prognostic marker in patients with osteosarcoma undergoing neoadjuvant chemotherapy (41). We have shown that ^{18}F Na imaging also allows the detection of osteoid formation in the primary tumor as well as in metastases and may provide valuable morphologic and prognostic information.

In this study, we characterize a preclinical model of osteosarcoma using clear-cut *in vivo* imaging techniques. These techniques (^{18}F FDG and $^{99\text{m}}\text{Tc}$ scintigraphies), which have been validated in patients (40, 41), provide a reliable, non-invasive, functional account of the tumor's behavior. Contrary to more conventional morphological methods, these techniques in our syngeneic orthotopic osteosarcoma model closely mimic its human counterpart, require fewer animals and can be repeated several times without major discomfort to the animal. Taken together our results show that this preclinical osteosarcoma model and the follow-up methods used in this study are relevant for the preclinical study of new drugs and innovative therapies.

Acknowledgements

This work was supported by a grant from La Ligue Nationale contre le Cancer (comité de la Haute Vienne). The authors would like to thank Jacques Démonet for excellent animal care.

References

- 1 Ferguson WS and Goorin AM: Current treatment of osteosarcoma. *Cancer Invest* 19: 292-315, 2001.
- 2 Ragland BD, Bell WC, Lopez RR and Siegal GP: Cytogenetics and molecular biology of osteosarcoma. *Lab Invest* 82: 365-373, 2002.
- 3 Kim JB, Stein R and O'Hare MJ: Three-dimensional *in vitro* tissue culture models of breast cancer – a review. *Breast Cancer Res Treat* 85: 281-291, 2004.
- 4 Kovar H, Ban J and Pospisilova S: Potentials for RNAi in sarcoma research and therapy: Ewing's sarcoma as a model. *Semin Cancer Biol* 13: 275-281, 2003.
- 5 Singh RK, Tsan R and Radinsky R: Influence of the host microenvironment on the clonal selection of human colon carcinoma cells during primary tumor growth and metastasis. *Clin Exp Metastasis* 15: 140-150, 1997.
- 6 Dutour A, Rabinovich-Chable H, Kaletta C, Michaelis U, Fiorenza F, Sturtz F and Rigaud M: Is troponin I gene therapy effective for osteosarcoma treatment? Study on a human-like orthotopic rat model. *Anticancer Res* 24: 3977-3982, 2004.
- 7 Indraccolo S, Gola E, Rosato A, Minuzzo S, Habeler W, Tisato V, Roni V, Esposito G, Morini M, Albini A, Noonan DM, Ferrantini M, Amadori A and Chieco-Bianchi L: Differential effects of angiostatin, endostatin and interferon-alpha(1) gene transfer on *in vivo* growth of human breast cancer cells. *Gene Ther* 9: 867-878, 2002.
- 8 Crnalic S, Hakansson I, Boquist L, Lofvenberg R and Brostrom LA: A novel spontaneous metastasis model of human osteosarcoma developed using orthotopic transplantation of intact tumor tissue into tibia of nude mice. *Clin Exp Metastasis* 15: 164-172, 1997.
- 9 Jia SF, Worth LL and Kleinerman ES: A nude mouse model of human osteosarcoma lung metastases for evaluating new therapeutic strategies. *Clin Exp Metastasis* 17: 501-506, 1999.
- 10 Shoieb AM, Hahn KA and Barnhill MA: An *in vivo/in vitro* experimental model system for the study of human osteosarcoma: canine osteosarcoma cells (COS31) which retain osteoblastic and metastatic properties in nude mice. *In Vivo* 12: 463-472, 1998.
- 11 Hiramoto RN, Ghanta VK and Lilly MB: Reduction of tumor burden in a murine osteosarcoma following hyperthermia combined with cyclophosphamide. *Cancer Res* 44: 1405-1408, 1984.
- 12 Joliat MJ, Umeda S, Lyons BL, Lynes MA and Shultz LD: Establishment and characterization of a new osteogenic cell line (MOS-J) from a spontaneous C57BL/6J mouse osteosarcoma. *In Vivo* 16: 223-228, 2002.
- 13 Suto R, Abe Y, Nakamura M, Ohnishi Y, Yoshimura M, Lee YH, Imanishi T, Yamazaki H, Kijima H, Tokunaga T, Oshika Y, Hiraoka N, Tamaoki N, Fukuda H and Ueyama Y: Multidrug resistance mediated by overexpression of P-glycoprotein in human osteosarcoma *in vivo*. *Int J Oncol* 12: 287-291, 1998.

- 14 Bodo A, Bakos E, Szeri F, Varadi A and Sarkadi B: The role of multidrug transporters in drug availability, metabolism and toxicity. *Toxicol Lett 140-141*: 133-143, 2003.
- 15 Preiss R: P-glycoprotein and related transporters. *Int J Clin Pharmacol Ther 36*: 3-8, 1998.
- 16 Vergote J, Moretti JL, de Vries EG and Garnier-Suillerot A: Comparison of the kinetics of active efflux of ^{99m}Tc-MIBI in cells with P-glycoprotein-mediated and multidrug-resistance protein-associated multidrug-resistance phenotypes. *Eur J Biochem 252*: 140-146, 1998.
- 17 Charissoux JL, Grossin L, Leboutet MJ and Rigaud M: Treatment of experimental osteosarcoma tumors in rat by *Herpes simplex* thymidine kinase gene transfer and ganciclovir. *Anticancer Res 19*: 77-80, 1999.
- 18 Dutour A, Monteil J, Paraf F, Charissoux JL, Kaletta C, Sauer B, Naujoks K and Rigaud M: Endostatin cDNA/cationic liposome complexes as a promising therapy to prevent lung metastases in osteosarcoma: study in a human-like rat orthotopic tumor. *Mol Ther 11*: 311-319, 2005.
- 19 Jasmin C, Allouche M, Jude JG, Klein B, Thiery JP, Perdereau B, Gongora R, Gongora G and Mazabraud A: An experimental model of osteosarcomas in rats . Article in french, *Sem Hop 58*: 1684-1689, 1982.
- 20 Allouche M, Delbruck HG, Klein B, Masse R, Matar A, Morin M, Lafuma J and Jasmin C: Malignant bone tumours induced by a local injection of colloidal radioactive ¹⁴⁴Cerium in rats as a model for human osteosarcomas. *Int J Cancer 26*: 777-782, 1980.
- 21 Carlsson G, Gullberg B and Hafstrom L: Estimation of liver tumor volume using different formulas – an experimental study in rats. *J Cancer Res Clin Oncol 105*: 20-23, 1983.
- 22 Declèves X, Regina A, Laplanche JL, Roux F, Boval B, Launay JM and Scherrmann JM: Functional expression of P-glycoprotein and multidrug resistance-associated protein (Mrp1) in primary cultures of rat astrocytes. *J Neurosci Res 60*: 594-601, 2000.
- 23 Kwan P, Sills GJ, Butler E, Gant TW and Brodie MJ: Differential expression of multidrug resistance genes in naive rat brain. *Neurosci Lett 339*: 33-36, 2003.
- 24 Provisor AJ, Ettinger LJ, Nachman JB, Krailo MD, Makley JT, Yunis EJ, Huvos AG, Betcher DL, Baum ES, Kisker CT and Miser JS: Treatment of nonmetastatic osteosarcoma of the extremity with preoperative and postoperative chemotherapy: a report from the Children's Cancer Group. *J Clin Oncol 15*: 76-84, 1997.
- 25 Asai T, Ueda T, Itoh K, Yoshioka K, Aoki Y, Mori S and Yoshikawa H: Establishment and characterization of a murine osteosarcoma cell line (LM8) with high metastatic potential to the lung. *Int J Cancer 76*: 418-422, 1998.
- 26 Khanna C, Prehn J, Yeung C, Caylor J, Tsokos M and Helman L: An orthotopic model of murine osteosarcoma with clonally related variants differing in pulmonary metastatic potential. *Clin Exp Metastasis 18*: 261-271, 2000.
- 27 Kjonniksen I, Winderen M, Bruland O and Fodstad O: Validity and usefulness of human tumor models established by intratibial cell inoculation in nude rats. *Cancer Res 54*: 1715-1719, 1994.
- 28 Cherrier B, Gouin F, Heymann MF, Thiery JP, Redini F, Heymann D and Duteille F: A new experimental rat model of osteosarcoma established by intrafemoral tumor cell inoculation, useful for biology and therapy investigations. *Tumour Biol 26*: 121-130, 2005.
- 29 Luu HH, Kang Q, Park JK, Si W, Luo Q, Jiang W, Yin H, Montag AG, Simon MA, Peabody TD, Haydon RC, Rinker-Schaeffer CW and He TC: An orthotopic model of human osteosarcoma growth and spontaneous pulmonary metastasis. *Clin Exp Metastasis 22*: 319-329, 2005.
- 30 Folkman J: What is the evidence that tumors are angiogenesis dependent? *J Natl Cancer Inst 82*: 4-6, 1990.
- 31 Gasparini G and Harris AL: Clinical importance of the determination of tumor angiogenesis in breast carcinoma: much more than a new prognostic tool. *J Clin Oncol 13*: 765-782, 1995.
- 32 Baldini N, Scotlandi K, Barbanti-Brodano G, Manara MC, Maurici D, Bacci G, Bertoni F, Picci P, Sottili S, Campanacci M and Serra M: Expression of P-glycoprotein in high-grade osteosarcomas in relation to clinical outcome. *N Engl J Med 333*: 1380-1385, 1995.
- 33 Burak Z, Moretti JL, Ersoy O, Sanli U, Kantar M, Tamgac F and Basdemir G: ^{99m}Tc-MIBI imaging as a predictor of therapy response in osteosarcoma compared with multidrug resistance-associated protein and P-glycoprotein expression. *J Nucl Med 44*: 1394-1401, 2003.
- 34 Chan HS, Grogan TM, Haddad G, DeBoer G and Ling V: P-glycoprotein expression: critical determinant in the response to osteosarcoma chemotherapy. *J Natl Cancer Inst 89*: 1706-1715, 1997.
- 35 Reynolds CP, Sun BC, DeClerck YA and Moats RA: Assessing growth and response to therapy in murine tumor models. *Methods Mol Med 111*: 335-350, 2005.
- 36 Hawkins DS, Rajendran JG, Conrad EU, III, Bruckner JD and Eary JF: Evaluation of chemotherapy response in pediatric bone sarcomas by [¹⁸F]-fluorodeoxy-D-glucose positron emission tomography. *Cancer 94*: 3277-3284, 2002.
- 37 Monteil J, Dutour A, Akla B, Chianea T, Le B, V, Grossin L, Paraf F, Petegnief Y, Vandroux JC, Rigaud M and Sturtz FG: *In vivo* follow-up of rat tumor models with 2-deoxy-2-[¹⁸F]-fluoro-D-glucose/dual-head coincidence gamma camera imaging. *Mol Imaging Biol 7*: 220-228, 2005.
- 38 Brenner W, Bohuslavizki KH and Eary JF: PET imaging of osteosarcoma. *J Nucl Med 44*: 930-942, 2003.
- 39 Schuetze SM: Utility of positron emission tomography in sarcomas. *Curr Opin Oncol 18*: 369-373, 2006.
- 40 Som P, Atkins HL, Bandoypadhyay D, Fowler JS, MacGregor RR, Matsui K, Oster ZH, Sacker DF, Shiue CY, Turner H, Wan CN, Wolf AP and Zabinski SV: A fluorinated glucose analog, 2-fluoro-2-deoxy-D-glucose (F-18): nontoxic tracer for rapid tumor detection. *J Nucl Med 21*: 670-675, 1980.
- 41 Ballinger JR: Imaging multidrug resistance with radiolabeled substrates for P-glycoprotein and multidrug resistance protein. *Cancer Biother Radiopharm 16*: 1-7, 2001.

Received May 2, 2007

Revised July 25, 2007

Accepted August 17, 2007